

Hadronic emission from the environment of the Crab Pulsar Wind Nebula by re-accelerated particles

S.T. Spencer^{1,2}, A.M.W. Mitchell¹ and B. Reville³

¹ Erlangen Centre for Astroparticle Physics (ECAP), Friedrich-Alexander-Universität Erlangen-Nürnberg, Nikolaus-Fiebiger-Str. 2, D 91058 Erlangen, Germany
e-mail: samuel.spencer@fau.de

² Department of Physics, Clarendon Laboratory, Parks Road, Oxford, OX1 3PU, United Kingdom

³ Max-Planck-Institut für Kernphysik, Saupfercheckweg 1, 69117 Heidelberg, Germany

Received September 15, 2001; accepted September 16, 3001

ABSTRACT

Context. The observation of peta-electronvolt (PeV) γ -ray photons from the Crab Nebula by LHAASO has revitalised the possibility of a secondary population of hadrons producing the highest energy emission through neutral pion decay. Despite previous studies modelling this population, the origin of such high-energy hadronic particles remains unclear.

Aims. We consider possible acceleration scenarios for multi PeV particles in the Crab Nebula environment, including one in which high-energy protons produced at the supernova remnant's outer shock diffuse into the pulsar wind nebula. Particles which reach the Crab Pulsar's wind termination shock can be accelerated to the required energies, and subsequently interact with the dense filaments surrounding the nebula.

Methods. We perform particle transport simulations of this scenario, including the effects of the expansion of the pulsar wind nebula into the surrounding supernova ejecta.

Results. We find that this results in PeV photons being produced over the lifetime of the Crab system, without over-estimating the flux at lower energies or exceeding the energy budget of the Crab Pulsar. This results in a reasonable match to the LHAASO data at the highest energies. We also present predictions for the resulting all-flavour neutrino flux, finding it to be approximately an order of magnitude below the sensitivity of current generation instruments.

Key words. astroparticle physics – γ rays: general – Neutrinos

1. Introduction

The Crab Nebula is the remnant of a star purported to have exploded in 1054 AD (Lundmark 1921). It is the most widely studied object in Very-High-Energy (VHE) γ -ray astrophysics, and was the first (and brightest persistent) TeV γ -ray source detected from the ground using the Imaging Atmospheric Cherenkov Telescope (IACT) technique (e.g. Weekes et al. 1989; Aharonian et al. 2004; Albert et al. 2008; Aharonian, F. et al. 2006). More recently, the γ -ray emission from the Crab Nebula has been found to have an extension of $(52.2 \pm 2.9_{\text{stat}} \pm 6.6_{\text{sys}})''$ at TeV energies in a H.E.S.S.-only analysis (H. E. S. S. Collaboration 2020), and $r_{68} = (0.82 \pm 0.29_{\text{stat}})'$ in a joint Fermi-LAT and H.E.S.S. analysis (Aharonian et al. 2024). The latter analysis found strong evidence for a decreasing size as a function of energy in the γ -ray regime up to ~ 100 TeV; the energy-dependent morphology in this range is likely lepton-dominated. Furthermore, pulsed emission from the central pulsar, PSR J0534+2200, has also been detected at TeV photon energies by MAGIC (Ansoldi, S. et al. 2016) and VERITAS (Nguyen & VERITAS Collaboration 2015). This pulsar is located at a distance of 2 kpc from Earth Kaplan et al. (2008), and has a spin down luminosity of 5×10^{38} erg s⁻¹ Smith et al. (2023).

As pointed out by Atoyan & Aharonian (1996), production of the TeV γ -ray emission purely via π^0 decay can be ruled out on energetic grounds. Thus, the primary emission mechanism for γ -rays above 100 GeV from the nebula is generally accepted

to be Inverse Compton (IC) scattering of photons in the nebula by energetic electrons and/or positrons. The target photons come from a variety of background radiation fields, though at photon energies above 100 TeV, the Cosmic Microwave Background (CMB) dominates (Cao et al. 2021). The wind termination shock (WTS) of the ultra-relativistic wind of the pulsar, located at ≈ 0.13 pc from the pulsar (Weisskopf et al. 2012), is thought to be the site of acceleration of the TeV emitting particles (e.g. Rees & Gunn 1974; Bell 1992; Amato & Arons 2006; Giacinti & Kirk 2018), though the details of the acceleration remain unclear. The magnetic field structure of the Crab Nebula has also recently been examined by the Imaging X-ray Polarimetry Explorer (IXPE) mission, revealing a predominantly toroidal magnetic field (Bucciantini et al. 2023), as expected for an oblique rotating pulsar (e.g. Coroniti 1990; Michel 1994; Bogovalov 1999).

Despite a purely hadronic origin for the GeV-TeV emission being ruled out, Atoyan & Aharonian (1996) proposed that a hard component could in principle dominate at higher energies. Such a scenario becomes increasingly favourable at ultra-high energies, where Klein-Nishina suppression will affect even CMB photons (e.g. Dirson & Horns 2023). The recent detection of PeV γ -ray emission by the Large High-Altitude Air Shower Observatory (LHAASO) (Cao et al. 2021) has re-opened this debate.

Previous studies exploring the role of hadronic emission in the context of the LHAASO results (e.g. Liu & Wang 2021; Peng et al. 2022; Nie et al. 2022), do not address the origin of the

multi-PeV particles required. However, even the processes underlying the energisation of inverse-Compton emitting particles are uncertain. It is broadly accepted that the pulsar wind termination shock plays the dominant role, though how exactly remains a topic of active investigation. Different models proposed include for example resonant cyclotron absorption of the pairs (e.g. Amato et al. 2003; Amato & Arons 2006) or directly via relativistic shock acceleration (Giacinti & Kirk 2018; Giacinti et al. 2022).

The resonant cyclotron absorption mechanism does not accelerate ions efficiently, but in order to produce the observed energetic pairs, it would require the pulsar wind to be energetically dominated by a cold ion component with a large bulk Lorentz factor $\Gamma_{\text{wind}} > 10^6$. Protons/ions embedded in such a wind, should they exist, would be thermalised at the shock and injected into the nebula at multi-PeV energies. Despite observational arguments supporting large bulk Lorentz factors (e.g. Kennel & Coroniti 1984b), whether they can be realised in practice remains uncertain (see Kirk et al. 2009, for a review)¹. If the ions are not energetically dominant, or the wind has a substantially lower bulk Lorentz factor, one could consider if relativistic shock acceleration can occur at the termination shock. Giacinti & Kirk (2018) have shown that particles of one charge can undergo multiple Fermi cycles at the shock in the equatorial region due to the field reversal across the equator. Both scenarios would require a non-negligible proton/nucleon component in the wind, whose presence is currently unconstrained (though see for example Bednarek & Protheroe 1997; Nie et al. 2022).

Alternative routes for PeV proton acceleration include diffusive shock acceleration at the outer blast wave of the supernova remnant associated to the progenitor of the Crab pulsar though favourable wind conditions of the progenitor star are needed for particles to exceed PeV energies (Bell et al. 2013). As pointed out by Bell (1992), lower energy protons accelerated at the outer shock can cross the nebula via a grad B drift, and interact with the relativistic termination shock of the pulsar wind (see also Lucek & Bell 1994; Bell & Lucek 1996; Ohira et al. 2018)

Global magneto-hydrodynamic (MHD) simulations of the Crab system predict a complex magnetic field topology in the enclosed PWN (Porth et al. 2014), through which particles can diffuse against the outward directed flow. We consider the possibility that protons accelerated earlier in the evolution of the forward shock of the SNR populate a reservoir of energetic particles in the region between the PWN boundary and the supernova forward shock. Following Bell (1992), we explore the possibility that particles of sufficiently high energy can in principle penetrate the nebula and reach the WTS. We apply a simple radial diffusion model, and do not consider the role of drift motions. There, protons can be re-accelerated, before escaping the nebula and subsequently re-interacting with gas in the reservoir. A schematic of our proposed scenario is shown in Figure 1. The existence of finger-like structures in the PWN seen in the infrared, believed to be caused by Rayleigh-Taylor instabilities at the PWN boundary, supports this hypothesis. Their presence suggests material is encroaching into the PWN from the surrounding SNR (Hester 2008). The goal of this work is to determine if this proposed scenario can account for the highest energy LHAASO γ -ray flux points reaching $\gtrsim 1$ PeV.

The outline of the remainder of this paper is as follows: in Section 2 we first make analytic estimates of the diffusion coefficient in the nebula and the resulting γ -ray flux. We then introduce the theory of an expanding PWN before introducing the

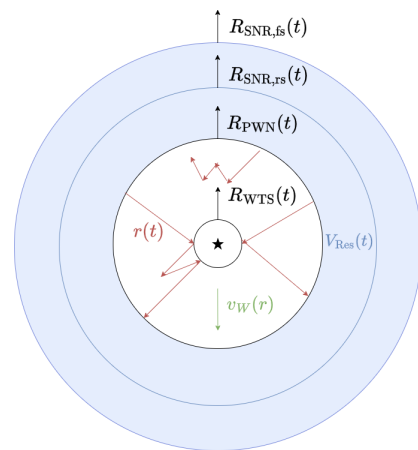


Fig. 1. Schematic of our proposed scenario, hadronic particles with position $r(t)$ (shown in red) are initially shocked by the SNR forward shock $R_{\text{SNR,fs}}$. They then travel from the reservoir region (volume V_{Res} , shown in blue) between the $R_{\text{SNR,fs}}$ and the pulsar wind nebula radius to the pulsar wind termination shock R_{WTS} . Following re-acceleration, they advect outwards with the pulsar wind (velocity v_W , shown by the green arrow) to hit the reservoir region they originated from. The black star denotes the pulsar’s position. For a system the age of the Crab, the supernova reverse shock $R_{\text{SNR,rs}}$ is still travelling outwards.

Monte-Carlo simulation procedure we adopt and our modelling of the resulting γ -ray emission. In Section 3 we compare the results of this modelling to the LHAASO data and to the available energy budget from the pulsar, before also making an estimate of the resulting neutrino flux. In Section 4 we present our conclusions.

2. Methods

2.1. Motivation and estimates

Working with the hypothesis that the γ -ray flux at and above PeV energies is dominated by hadronic emission, the LHAASO flux of $\phi(E_\gamma > 10^{15} \text{ eV}) \gtrsim 10^{-14} \text{ erg/cm}^2/\text{s}$ can be used to constrain the total energy of protons and other nuclei to be $w_{\text{tot}}(E > \text{PeV}) \approx 10^{46}/\langle n_H \rangle \text{ erg}$, irrespective of the acceleration process. Here $\langle n_H \rangle$ is the average gas target density surrounding the nebula. This can be compared against the kinetic energy provided by the supernova of $E_{\text{SNR}} \approx 10^{51} \text{ erg}$, or the integrated energy released by the central pulsar $E_{\text{pulsar}} \gg 10^{49} \text{ erg}$. The latter inequality assumes the spin-down power was larger in the past. It is evident that a modest efficiency of less than a fraction of a percent would be sufficient in either scenario to account energetically for the required PeV protons.

Modelling the multi-wavelength observations of the Crab PWN generally indicate that the root mean square field inside the nebula is $B_{\text{PWN}} \approx 100 \mu\text{G}$. The transport of energetic particles in this field is sensitive to both its global topology and the details of the MHD turbulence embedded in the flow. Based on recent X-ray polarisation measurements (Bucciantini et al. 2023), it appears that the radial component of the field is subdominant in the nebula and thus the radial diffusion coefficient should not exceed the Bohm limit. Adopting present-day parameters for the nebula, one can estimate an upper limit on the radial diffusion length of $r_{\text{diff}}(\text{PeV}) < \sqrt{4\kappa_{\text{Bohm}} t} \approx 2B_{100\mu\text{G}}^{-1/2} t_{\text{kyr}}^{1/2} \text{ pc}$, i.e. comparable to the expected present-day radius of the nebula. This is consistent with the results of 3D MHD simulations of radial diffusion in the Crab Nebula by Porth et al. (2016),

¹ see also Kirk & Giacinti (2019) for a study of the impact of protons on the Crab pulsar wind.

who found an almost energy independent radial diffusion coefficient of $\lesssim 10^{27} \text{ cm}^2 \text{ s}^{-1}$ for test particles with Lorentz factors $\gamma \ll 10^{10}$. For such small radial diffusion, ions that recently interacted with the wind termination shock remain inside the nebula, while those entering the nebula from outside at the current epoch have a negligible probability of reaching the wind termination shock through diffusion alone (in this work, we do not consider drift motions as done in Bell 1992). Knowledge of the time history and internal structure of the supernova remnant are therefore important for hadronic models of the PeV γ -ray emission.

As mentioned in the introduction, we consider the possibility that, during the early stages of the SNR expansion, a fraction of the energy processed by the forward shock was converted to cosmic rays. The particles that accumulate downstream of the external shock enclose the pulsar wind nebula, forming a reservoir of relativistic ions which for simplicity we assume to be comprised exclusively of protons. According to the standard CR-SNR origins model (e.g. Ginzburg & Syrovatskii 1964) approximately 10% of the SNR's kinetic energy should be converted to CRs over its lifetime. Given the relatively young age of the Crab pulsar, we do not expect the total energy in the reservoir to exceed this.

It is possible to constrain the total energy, by requiring that emission from the reservoir does not dominate over the inverse-Compton emission from the nebula, at sub PeV energies. This is also a consistency check of our proposed model. Assuming the non-thermal proton distribution in the reservoir is a power-law, $dN/dE \propto E^{-s}$ above 1 GeV, the γ -ray flux at earth is approximately

$$\Phi = E_\gamma^2 \frac{dN_\gamma}{dE_\gamma dt dA} \approx 10^{-12} \left(\frac{D}{2 \text{ kpc}} \right)^{-2} \left(\frac{\eta}{10^{-4}} \right) \left(\frac{E_{\text{SN}}}{10^{51}} \right) \left(\frac{n_H}{10 \text{ cm}^{-3}} \right) \left(\frac{E_\gamma}{\text{GeV}} \right)^{2-s} \frac{\text{erg}}{\text{cm}^2 \text{ s}},$$

where we introduce the efficiency parameter η as the fraction of the total kinetic energy of the SNR in CRs above a GeV, $w_{\text{tot}}(E > \text{GeV}) = \eta E_{\text{SN}}$. For the above numerical values, assuming $s \gtrsim 2$ and that the cut-off in the proton distribution extends well beyond several PeV, this alone could accommodate the LHAASO measurements. While this cannot be ruled out based on current observational constraints, it requires that the SNR shock both accelerates and confines particles well beyond a PeV inside the remnant, which is a challenge for current theoretical models (Bell et al. 2013).

If on the other hand protons accelerated at the SNR's external shock reach some maximum energy \ll PeV, these CRs could fill the volume between the PWN and the outer SNR shock with the desired reservoir. The resulting hadronic emission from these particles would cut off below the LHAASO energy range, with flux level negligible compared to the inverse Compton emission. Similar arguments can be used to rule out a dominant leptonic contribution from the SNR.

2.2. PWN evolution

For the spherically symmetric evolution of the system, we follow the approach of van der Swaluw et al. (2001). In their model, the PWN radius satisfies

$$R_{\text{PWN}}(t) = 1.04 \left(\frac{\dot{E} t_S}{E_{\text{SN}}} \right)^{1/5} \left(\frac{t}{t_S} \right)^{6/5} R_S, \quad (1)$$

where, R_S is the Sedov radius given by

$$R_S = 0.805 t_S \left(\frac{10 E_{\text{SN}}}{M_{\text{ej}}} \right), \quad (2)$$

and $E_{\text{SN}} = 10^{51} \text{ erg}$ is the supernova energy and $M_{\text{ej}} = 3 M_\odot$ is the supernova ejecta mass. Assuming an ISM density of $n = 0.1 \text{ cm}^{-3}$, t_S is the Sedov time given by $t_S \approx 10^3 \text{ yr}$ in this case. The velocity of the outer radius of the PWN, v_{PWN} , as a function of time is given by dR_{PWN}/dt ,

$$v_{\text{PWN}} = 1.04 \times \frac{6}{5} \left(\frac{\dot{E} t_S}{E_{\text{SN}}} \right)^{1/5} \left(\frac{R_S}{t_S} \right) \left(\frac{t}{t_S} \right)^{1/5} \quad (3)$$

for the current stage of the Crab's evolution. The WTS radius is fixed as 5% of the PWN radius at each timestep such that the size of the WTS at the current time is approximately correct (0.1 pc).

2.3. Simulation procedure

We seek to determine what fraction of the particles in the CR reservoir can interact with the WTS, and be accelerated there to higher energies. This requires a number of assumptions on the nature of the particle transport in the nebula, and the acceleration process itself. Analytic treatments of particle acceleration at relativistic shocks is complicated by the fact that the ratio of the shock velocity to the speed of light is not a small parameter that can be exploited (see for example Kirk et al. 2023). To proceed we make a number of simplifying assumptions. We assume the system is spherically symmetric, and that it can be approximately treated with the non-relativistic transport equation:

$$\frac{\partial f}{\partial t} + u_r \frac{\partial f}{\partial r} = \frac{1}{r^2} \frac{\partial}{\partial r} \left[r^2 \kappa \frac{\partial f}{\partial r} \right] + \frac{1}{3r^2} \frac{\partial r^2 u_r}{\partial r} p \frac{\partial f}{\partial p}, \quad (4)$$

where $f(r, p, t)$ is the isotropic part of the distribution function, $u_r(r)$ the radial fluid velocity, and κ the radial diffusion coefficient. In general, equation (4) requires that the distribution remains close to isotropic, and the flow satisfies $u_r \ll c$, both of which break down in the vicinity of the relativistic shock. We discuss how we avoid this complication below.

Defining $F = 4\pi p^3 4\pi r^2 f$, Eq. (4) can be recast in the form:

$$\frac{\partial F}{\partial t} + \frac{\partial}{\partial r} \left[u_{\text{eff}} F - \frac{\partial}{\partial r} (\kappa F) \right] - \frac{\partial}{\partial y} \left[\frac{1}{r^2} \frac{\partial r^2 u_r}{\partial r} F \right] = 0 \quad (5)$$

where $u_{\text{eff}}(r) = u_r + \frac{1}{r^2} \frac{\partial(r^2 \kappa)}{\partial r}$ is the effective radial velocity and $y = \ln(E/E_0)$. We choose $E_0 = 1 \text{ GeV}$. For simplicity, we further assume κ is constant and uniform in the nebula, and has Bohm scaling

$$\kappa = \frac{1}{3} \beta r_g c = \beta \left(\frac{E c}{3e B_{\text{max}}} \right), \quad (6)$$

where r_g is the particle gyroradius, E its energy, B_{max} is the magnetic field strength and β a free parameter which we set to unity. We set the magnetic field strength to be $112 \mu\text{G}$ in order to reproduce the synchrotron and IC emission from X-ray wavelengths to PeV at the current epoch with single-zone models (Cao et al. 2021).

Equation (5) is of the standard Fokker-Planck form, which readily lends itself to a Stochastic Differential Equation approach (e.g. Gardiner 1994; Achterberg & Krulls 1992; Marcowith & Kirk 1999), whereby a large number of pseudo-particles are integrated in time, generating a particle distribution

that is equivalent to that produced by the Fokker-Planck equation.

Particles are continuously injected at the outer surface of the PWN, at $r = R_{\text{PWN}}(t)$. The region between the PWN and the rest of the SNR interior is assumed to be a uniform reservoir of cosmic rays with energy density $\langle u_{\text{cr}} \rangle = \eta E_{\text{SN}}/V_{\text{Res}}$, where $V_{\text{Res}} = \frac{4\pi}{3}(R_{\text{SNR,fs}}(t)^3 - R_{\text{PWN}}(t)^3)$ is the reservoir's volume. For simplicity, we take as $R_{\text{SNR,fs}}(t)$ the solution of McKee & Truelove (1995). Both V_{res} and η are in reality time dependent, though since we do not know the history of the external medium in the early stages of the SNR, nor the CR escape history, we take η to be a fixed value.

The energy distribution of CRs in the reservoir is taken to be a power-law $F \propto (E/E_0)^{-S}$, with $S > 1$, where we consider that the particles likely to be re-accelerated have energies between the limits $E_1 = 1$ TeV and $E_2 = 50$ TeV. Particles are injected at each time step, chosen in such a way that the integrated energy density matches that in the reservoir. This implies a numerical weighting factor for each macro-particle of $\alpha \left(\frac{E}{E_0}\right)^{-S}$, where we inject N_{inj} macro-particles at each timestep, logarithmically spaced between and $\ln(E_1/E_0)$ and $\ln(E_2/E_0)$, such that α is given by

$$\alpha = \frac{4\pi R_{\text{PWN}}^2}{(N_{\text{inj}} - 1)} (S - 1) \ln(E_2/E_1) \left(\frac{\eta E_{\text{SN}}}{E_0}\right) \left(\frac{v_{\text{PWN}} \Delta t}{V_{\text{res}}(t)}\right). \quad (7)$$

For the results presented, the number of macro-particles injected per time step is $N_{\text{inj}} = 2000$. The evolution of α over time is shown in Figure 2.

The evolution of the injected particles are evolved using a standard SDE formalism. At each timestep, each pseudo-particle's radius r is updated such that

$$\Delta r = u_{\text{eff}} \Delta t + \xi_R \sqrt{2\kappa \Delta t}, \quad (8)$$

where ξ_R is a random number following a standard normal distribution centred at zero with a standard deviation of unity.

The flow profile in the nebula is chosen to satisfy

$$u_r(r) = \frac{c}{3} \left(\frac{R_{\text{WTS}}}{r}\right)^2, \quad (9)$$

following the low magnetisation wind bubble solution (Weaver et al. 1977) (see also Kennel & Coroniti 1984a). Since u_r is divergence free, no change occurs in the particles' energy during any timestep unless the diffusive step results in a pseudo-particle crossing the internal WTS boundary. As stated earlier, the transport equation cannot capture the physics near the shock. We circumvent this issue by simply doubling the particle's energy (as is expected at an ultra-relativistic shock, see Achterberg et al. 2001) and reflect its position downstream such that $r_{\text{new}} = R_{\text{WTS}} + |R_{\text{WTS}} - r_{\text{old}}|$. Note that for Bohm diffusion, the effective radial velocity for any particle on the shock surface is

$$\frac{u_{\text{eff}}}{c} = \frac{1}{3} + \frac{2r_g}{3R_{\text{WTS}}} < 1 \quad \text{for } r_g < R_{\text{WTS}}. \quad (10)$$

Since $r_g = R_{\text{WTS}}$ corresponds to the Hillas limit for relativistic shocks (Hillas 1984), this condition is satisfied. Provided the time step is chosen such that $\sqrt{2\kappa \Delta t} < c \Delta t$, the maximum energy cannot exceed the Hillas limit, since radial outward directed advection must exceed the diffusive step. For our chosen values, the Hillas limit is $E_{\text{Hillas}} \approx 10^{16}$ eV for protons.

The free parameters used in the simulation are shown in Table 1. The computational domain only covers the region $r_{\text{WTS}} <$

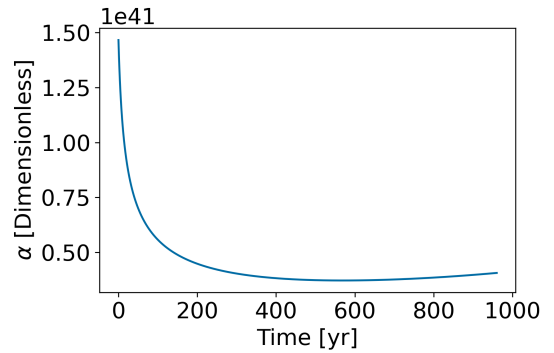


Fig. 2. Values of α at injection over the duration of the simulation. α (determined by Equation 7) is assigned to each particle at injection and acts as a weighting factor in the particle spectrum upon escape.

$r < r_{\text{PWN}}$. Any particle that is transported outside the domain ($r > r_{\text{PWN}}$) is recorded, only if it has interacted with the WTS at least once. These particles are injected back into the reservoir and assumed to remain there.

2.4. γ -ray spectrum

The package GAMERA (Hahn 2015; Hahn et al. 2022) is used to infer the γ -ray spectrum from the protons interacting with the reservoir using the cross-section parameterisations of Kafexhiu et al. (2014). The reservoir is taken as a static target with a 5 cm^{-3} density, with the proton spectra from the simulation at 969 years being used as the input proton distribution. It should be noted that the normalisation of the hadronic spectrum here is effectively a free parameter given the assumptions about the density in the target material and the fraction of the supernova energy in the population of re-accelerated hadrons. To model the hadronic emission, we employed the SYBIL 2.1 (Ahn et al. 2009) code as supported by GAMERA.

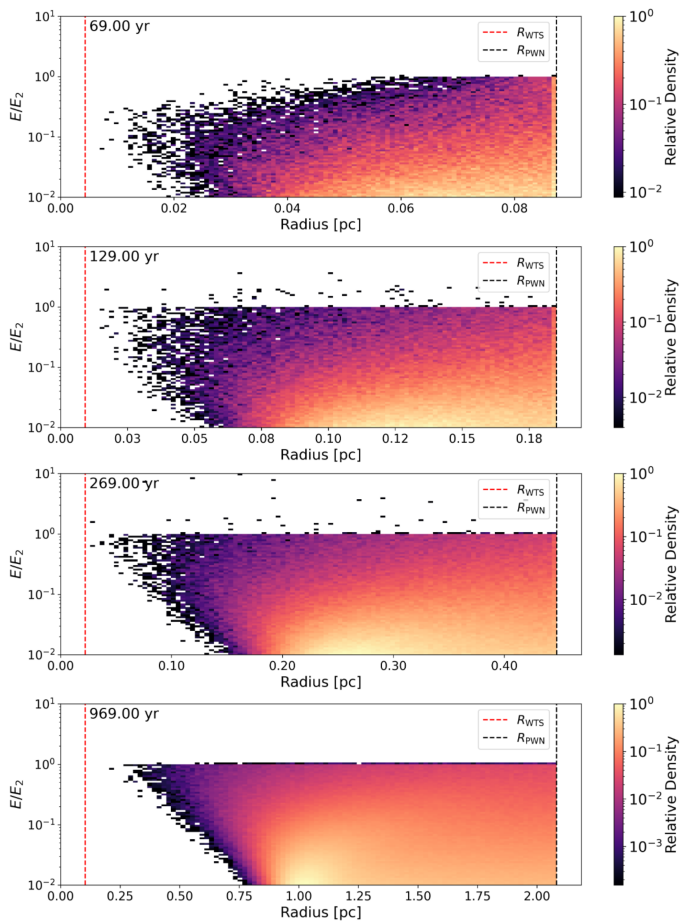
3. Results and discussion

3.1. Comparison to γ -ray data

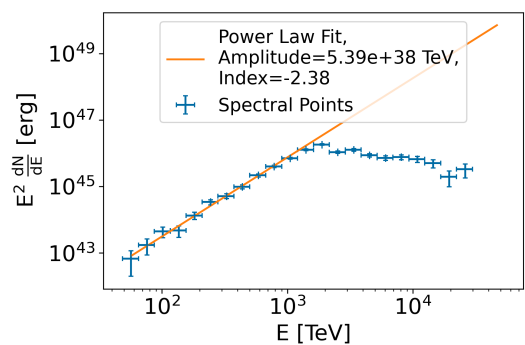
Figure 3 shows instantaneous steps of our simulations at selected times, which particle energy relative to the maximum injection energy as a function of radius from the pulsar. This shows that the majority of re-accelerated particles interact with the WTS comparatively early (with the first interactions occurring around 30 years), before advecting outwards with the wind. The majority of interactions occur at approximately ~ 100 years. After ~ 650 years the simulations effectively freeze-out, with no high energy particles being shocked or remaining within the PWN, as expected. These results further indicate that protons re-accelerated at the WTS are, as anticipated, outliers. If the contrary were true, their emission would potentially exceed the observed flux at lower energies. A secondary population of electrons and positrons produced through the secondary hadronic population's proton-proton interactions would not be detectable above the existing inverse Compton emission from the primary electrons. Figure 4 shows the spectrum of re-accelerated protons that exit the PWN and merge with the CR reservoir; a clear break at ~ 1 PeV is seen. The resulting γ -ray spectrum is found using GAMERA, and is compared to the LHAASO flux points in Figure 5. Here the multi-band leptonic model fit from Dirson & Horns (2023) is taken for the IC component. Our re-acceleration model provides a reasonable match to the data, in-

Table 1. Fixed parameters set in the simulation with associated values based on previous literature.

Parameter	Description	Value	Notes
t_0	Simulation start time	9 years	-
t_{end}	Simulation end time	969 years	Stephenson & Green (2003)
B_{Max}	Maximum magnetic field strength in PWN	112 μG	Cao et al. (2021)
Δt	Timestep	0.01 years	Based on constraints from Liu & Wang (2021).
M_{ej}	Mass ejected in supernova	$5M_{\odot}$	Fesen et al. (1997)
E_{SN}	Supernova energy	10^{51} erg	-
η	Fraction of E_{SN} in protons in the reservoir	7×10^{-5}	-
E_0	Proton normalisation energy	1 GeV	-
\dot{E}	Spin-down luminosity of Crab pulsar at current time	5×10^{38} erg s^{-1}	Hester (2008)
n_{ISM}	Proton density in ISM	0.1 cm^{-3}	-
n_{Target}	Proton density in target material	5 cm^{-3}	-
D	Distance to Crab nebula	2 kpc	Kaplan et al. (2008)
β	Diffusion coefficient relative to Bohm diffusion	1	-
N_{inj}	Pseudo-particles injected per timestep	2000	-
E_1	Minimum pseudo-particle injection energy	1 TeV	-
E_2	Maximum pseudo-particle injection energy	50 TeV	-
S	Pseudo-particle injection spectral index	1.2	-


Fig. 3. Instantaneous steps of the simulation over time. At each time step, the distribution of particle energies compared to the maximum injection particle energy is shown as function of distance from the pulsar. A small number of particles with energy ratios greater than 1 can be seen, corresponding to interactions with the WTS. The PWN radius is constrained to reach the current size at the end of the simulation, 969 yrs. At late times (≥ 650 years), there are no interactions with the WTS and very few shocked particles remain within the nebula.

dicating that a hadronic re-acceleration scenario cannot be excluded as the origin of the highest energy emission. A longer integration time with LHAASO or next-generation detectors such as the Cherenkov Telescope Array Observatory (CTAO) will


Fig. 4. Spectrum of re-accelerated protons that have escaped the PWN at the final timestep, the Poisson errors on these measurements are shown, the x -axis errors denote the size of the bins. A power-law fit of $E^2 dN/dE$ up to 1 PeV, normalised to 1 TeV, is shown for comparison to highlight the spectral break.

help to constrain this hadronic scenario further. In particular, the improved angular resolution of CTAO ($\sim 0.02^\circ$ at 100 TeV) could help determine if the highest energy γ -rays are correlated with the position of the target gas that sits outside the nebula (CTAO and CTAO Consortium 2021). A very small number of particles (~ 10 s out of $\sim 10^8$ injected) interacting with the shock > 10 times appears to be able to account for the highest energy emission, this can be seen in Figure 6. These tend to be the particles injected with lower energies as a result of the statistics of the injection. To confirm that the pulsar can provide sufficient power to re-accelerate the protons, we compare the energy gained by the pseudo-particles at the WTS to the pulsar spin-down luminosity of the pulsar $\dot{E}(t)$ over time

$$\dot{E}(t) = \dot{E}_0 \left(1 + \frac{t}{\tau_0} \right)^{-\frac{(n+1)}{(n-1)}}, \quad (11)$$

where \dot{E}_0 is the spin-down luminosity at birth and n is the braking index (which we fix to be 2). The characteristic age of the pulsar τ_0 is given by

$$\tau_0 = \frac{P_0}{(n-1)\dot{P}_0} \quad (12)$$

where we take the values from Zhang et al. (2020) for the Crab pulsar birth period $P_0 = 18.3$ ms and birth period derivative $\dot{P}_0 =$

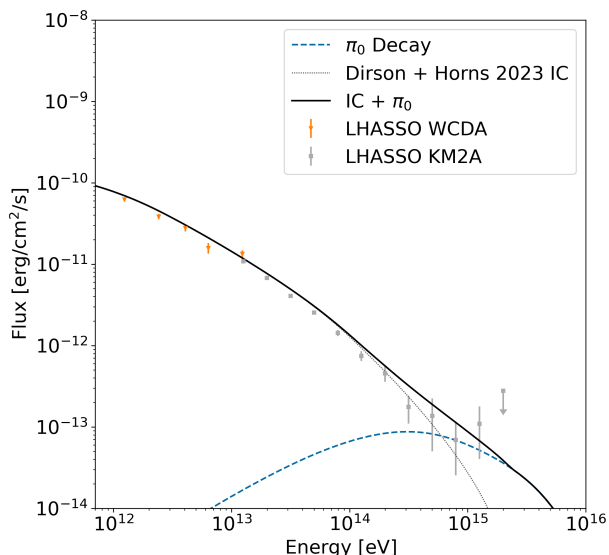


Fig. 5. Hadronic Crab spectra as modelled using GAMERA with SIBYLL 2.1. The Inverse Compton spectra from Dirson & Horns (2023) is also shown.

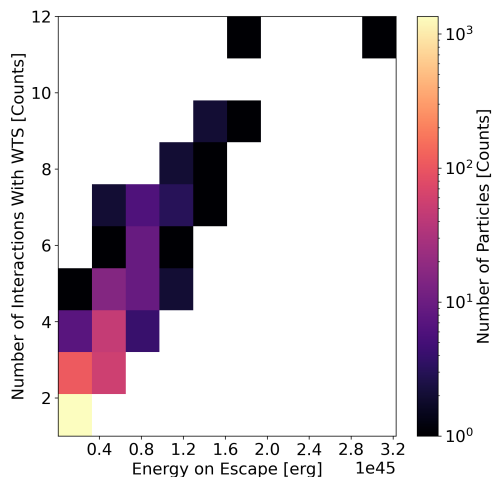


Fig. 6. Re-weighted particle energies on escape from the PWN as a function of the number of interactions with the WTS. Only a small number of the $\sim 10^8$ total particles injected over the PWN’s history ever reach the WTS, of which a few 10s can interact with the shock $\gtrsim 10$ times.

$6.4 \times 10^{-13} \text{ s s}^{-1}$. To calculate \dot{E}_0 we use the equation

$$\dot{E}_0 = 4\pi^2 I \frac{\dot{P}_0}{P_0^3} \quad (13)$$

(c.f. Gaensler & Slane 2006), where $I = 10^{45} \text{ g cm}^2$ is the neutron star’s moment of inertia. The results of this comparison are shown in Figure 7. In order to match the highest energy LHAASO flux point, we select η to be 7×10^{-5} . This suggests that in our scenario only a small portion of the pulsar’s spin-down luminosity would ultimately go into the re-acceleration of CRs. We also performed simulations with S in the range 1.1-1.3, and with E_2 as 25 TeV and 75 TeV; the effect on the spectrum was minor and would not change our conclusions, especially given the freedom of the selected value of η .

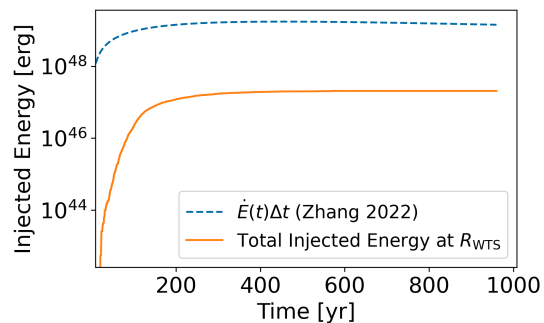


Fig. 7. The spin-down energy output of the pulsar compared to the total energy injected by the pulsar into re-accelerated hadrons at the WTS.

3.2. Predicted neutrino flux

The neutrino flux we predict from our secondary hadronic population, according to the prescription of Kelner et al. (2006) is shown in Figure 8. Similar to Peng et al. (2022), we find that the predicted neutrino flux is substantially below the sensitivity threshold of current generation instruments such as the IceCube neutrino observatory (IceCube Collaboration 2023) and the upcoming KM3Net neutrino detector (Adrián-Martínez et al. 2016). This could potentially be in tension with the hotspot associated with the Crab in the recent cascade event analysis performed by the IceCube collaboration IceCube Collaboration (2023).

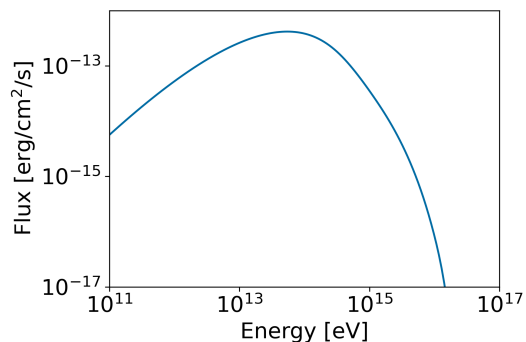


Fig. 8. Neutrino flux prediction for our re-acceleration model, for reference the current generation of neutrino detectors have an optimal sensitivity at 100 TeV of approximately $10^{-12} \text{ erg cm}^{-2} \text{ s}^{-1}$ (Aartsen et al. 2019).

4. Conclusions

In this work we have performed particle transport simulations to discern whether the highest energy emission from the Crab Nebula as observed by LHAASO could have a hadronic contribution, assuming a physically motivated re-acceleration scenario. Our work shows that, in principle, protons have sufficient time to travel from the region between the PWN radius and the SNR forward shock to the WTS, interact multiple times with the WTS region, and travel back again. Our model provides a reasonable quality match to the LHAASO data without over-estimating the flux at lower energies, indicating that a hadronic scenario cannot be excluded. Our results motivate further, more realistic 3D simulations to continue exploring this scenario. Possible extensions of this model could take into account the reverberation phase in older systems, in which the combination of crushing of the PWN

by the SNR reverse shock (Ohira et al. 2018) and re-acceleration at the central WTS could lead to PeV particles being produced in greater numbers.

Acknowledgements. S. Spencer and A. Mitchell are supported by the Deutsche Forschungsgemeinschaft (DFG, German Research Foundation) – Project Number 452934793.

References

- Aartsen, M. G., Ackermann, M., et al. 2019, *The European Physical Journal C*, 79
- Achterberg, A., Gallant, Y. A., Kirk, J. G., & Guthmann, A. W. 2001, *Monthly Notices of the Royal Astronomical Society*, 328, 393
- Achterberg, A. & Krulls, W. M. 1992, *A&A*, 265, L13
- Adrián-Martínez, S., Ageron, M., Aharonian, F., et al. 2016, *Journal of Physics G: Nuclear and Particle Physics*, 43, 084001
- Aharonian, F., Akhperjanian, A., Beilicke, M., et al. 2004, *ApJ*, 614, 897
- Aharonian, F., Benkhali, F. A., Aschersleben, J., et al. 2024, *Spectrum and extension of the inverse-Compton emission of the Crab Nebula from a combined Fermi-LAT and H.E.S.S. analysis*
- Aharonian, F., Akhperjanian, A. G., Bazer-Bachi, A. R., et al. 2006, *A&A*, 457, 899
- Ahn, E.-J., Engel, R., Gaisser, T. K., Lipari, P., & Stanev, T. 2009, *Physical Review D*, 80
- Albert, J., Aliu, E., Anderhub, H., et al. 2008, *ApJ*, 674, 1037
- Amato, E. & Arons, J. 2006, *ApJ*, 653, 325
- Amato, E., Guetta, D., & Blasi, P. 2003, *Astronomy & Astrophysics*, 402, 827–836
- Ansoldi, S., Antonelli, L. A., Antoranz, P., et al. 2016, *A&A*, 585, A133
- Atoyan, A. M. & Aharonian, F. A. 1996, *Monthly Notices of the Royal Astronomical Society*, 278, 525
- Bednarek, W. & Protheroe, R. J. 1997, *Phys. Rev. Lett.*, 79, 2616
- Bell, A. R. 1992, *MNRAS*, 257, 493
- Bell, A. R. & Lucek, S. G. 1996, *MNRAS*, 283, 1083
- Bell, A. R., Schure, K. M., Reville, B., & Giacinti, G. 2013, *MNRAS*, 431, 415
- Bogovalov, S. V. 1999, *A&A*, 349, 1017
- Bucciantini, N., Ferrazzoli, R., Bachetti, M., et al. 2023, *Nature Astronomy*, 7, 602
- Cao, Z. et al. 2021, *Science*, 373, 425–430
- Coroniti, F. V. 1990, *ApJ*, 349, 538
- CTAO and CTAO Consortium. 2021, *CTAO Instrument Response Functions - prod5 version v0.1*
- Dirson, L. & Horns, D. 2023, *A&A*, 671, A67
- Fesen, R. A., Shull, J. M., & Hurford, A. P. 1997, *AJ*, 113, 354
- Gaensler, B. M. & Slane, P. O. 2006, *Annual Review of Astronomy and Astrophysics*, 44, 17–47
- Gardiner, C. W. 1994, *Handbook of stochastic methods for physics, chemistry and the natural sciences* (Springer)
- Giacinti, G. & Kirk, J. G. 2018, *The Astrophysical Journal*, 863, 18
- Giacinti, G., Reville, B., & Kirk, J. 2022, in *37th International Cosmic Ray Conference*, 913
- Ginzburg, V. L. & Syrovatskii, S. I. 1964, *The Origin of Cosmic Rays* (Macmillan, New York)
- H. E. S. S. Collaboration. 2020, *Nature Astronomy*, 4, 167
- Hahn, J. 2015, in *GAMERA - A Modular Framework For Spectral Modeling In VHE Astronomy*
- Hahn, J., Romoli, C., & Breuhaus, M. 2022, *GAMERA: Source modeling in gamma astronomy*, *Astrophysics Source Code Library*, record ascl:2203.007
- Hester, J. J. 2008, *ARA&A*, 46, 127
- Hillas, A. M. 1984, *ARA&A*, 22, 425
- IceCube Collaboration. 2023, *Science*, 380, 1338
- Kafexhiu, E., Aharonian, F., Taylor, A. M., & Vila, G. S. 2014, *Phys. Rev. D*, 90, 123014
- Kaplan, D. L., Chatterjee, S., Gaensler, B. M., & Anderson, J. 2008, *The Astrophysical Journal*, 677, 1201
- Kelner, S. R., Aharonian, F. A., & Bugayov, V. V. 2006, *Phys. Rev. D*, 74, 034018
- Kennel, C. F. & Coroniti, F. V. 1984a, *ApJ*, 283, 694
- Kennel, C. F. & Coroniti, F. V. 1984b, *ApJ*, 283, 710
- Kirk, J. G. & Giacinti, G. 2019, *ApJ*, 884, 62
- Kirk, J. G., Lyubarsky, Y., & Petri, J. 2009, in *Astrophysics and Space Science Library*, Vol. 357, *Astrophysics and Space Science Library*, ed. W. Becker, 421
- Kirk, J. G., Reville, B., & Huang, Z.-Q. 2023, *MNRAS*, 519, 1022
- Liu, R.-Y. & Wang, X.-Y. 2021, *The Astrophysical Journal*, 922, 221
- Lucek, S. G. & Bell, A. R. 1994, *MNRAS*, 268, 581
- Lundmark, K. 1921, *Publications of the Astronomical Society of the Pacific*, 33, 225
- Marcowith, A. & Kirk, J. G. 1999, *A&A*, 347, 391
- McKee, C. F. & Truelove, J. K. 1995, *Phys. Rep.*, 256, 157
- Michel, F. C. 1994, *ApJ*, 431, 397
- Nguyen, T. & VERITAS Collaboration. 2015, in *International Cosmic Ray Conference*, Vol. 34, *34th International Cosmic Ray Conference (ICRC2015)*, 828
- Nie, L., Liu, Y., Jiang, Z., & Geng, X. 2022, *The Astrophysical Journal*, 924, 42, publisher: The American Astronomical Society
- Ohira, Y., Kisaka, S., & Yamazaki, R. 2018, *Monthly Notices of the Royal Astronomical Society*, 478, 926
- Peng, Q.-Y., Bao, B.-W., Lu, F.-W., & Zhang, L. 2022, *The Astrophysical Journal*, 926, 7, publisher: The American Astronomical Society
- Porth, O., Komisarov, S. S., & Keppens, R. 2014, *MNRAS*, 438, 278
- Porth, O., Vorster, M. J., Lyutikov, M., & Engelbrecht, N. E. 2016, *MNRAS*, 460, 4135
- Rees, M. J. & Gunn, J. E. 1974, *MNRAS*, 167, 1
- Smith, D. A., Abdollahi, S., Ajello, M., et al. 2023, *ApJ*, 958, 191
- Stephenson, F. R. & Green, D. A. 2003, *Journal of Astronomical History and Heritage*, 6, 46
- van der Swaluw, E., Achterberg, A., Gallant, Y. A., & Tóth, G. 2001, *A&A*, 380, 309
- Weaver, R., McCray, R., Castor, J., Shapiro, P., & Moore, R. 1977, *ApJ*, 218, 377
- Weekes, T. C., Cawley, M. F., Fegan, D. J., et al. 1989, *ApJ*, 342, 379
- Weisskopf, M. C., Elsner, R. F., Kolodziejczak, J. J., O’Dell, S. L., & Tennant, A. F. 2012, *ApJ*, 746, 41
- Zhang, X., Chen, Y., Huang, J., & Chen, D. 2020, *Monthly Notices of the Royal Astronomical Society*, 497, 3477